A Self-Consistent Semi-Analytical Model for AlGaAs/InGaAs PMHEMTs

M. Abdel Aziz, M. El-Banna, and M. El-Sayed

Abstract — **A semi-analytical model based on exact numerical analysis of the 2DEG channel in pseudo-morphic HEMT (PMHEMT) is presented. The exactness of the model stems from solving both Schrodinger's wave equation and Poisson's equation simultaneously and self-consistently. The analytical modeling of the device terminal characteristics in relation to the charge control model has allowed a best fit with the geometrical and structural parameters of the device. The numerically obtained data for the charge control of the channel are best fitted to analytical expressions which render the problem analytical. The obtained good agreement between experimental and modeled current/voltage characteristics and small signal parameters has confirmed the validity of the model over a wide range of biasing voltages. The model has been used to compare both the performance and characteristics of a PMHEMT with a competetive HEMT. The comparison between the two devices has been made in terms of 2DEG density, transfer characteristics, transconductance, gate capacitance and unity current gain cut-off frequency. The results show that PMHEMT outperforms the conventional HEMT in all considered parameters.**

Index Terms — **Interconnects, Doplanar strip line, Fourier series approach, silicon substrate, point matching procedure.**

Manuscript received February 25, 2002; revised March 12, 2002.
Department Faculty of Engineering Alexandria University .
(e-mail : mbanna@dataxprs.com.eg)Tel : +203-549-8108

1. INTRODUCTION

High Electron Mobility Transistors, HEMTs, based on AlGaAs/GaAs heterostructure have shown rapid progress in microwave and digital applications. Performance superior to those structures has been achieved using AlGaAs/InGaAs pseudomorphic HEMT (PMHEMT), where higher electron velocity and better carrier confinement have been obtained by the incorporation of indium in the heterostructure. New record values for the device extrinsic transconductance g_{mext} and current-gain cutoff frequency f_T are reported ($g_{mext} = 1070\ mS/mm$ and $f_T = 220\ GHz$ [1]).

An important parameter in modulation doped tructures is the conduction band discontinuity (ΔE_C) between the higher bandgap material and the channel layer material. A small discontinuity results in less efficient electron transfer, and therefore smaller 2DEG concentration, as well as in less electron confinement inside the potential well, and hence, reduced electron mobility. Moreover, a small ΔE_C leads to an increased probability of undesired MESFET conduction [2], and a possibility of hot-electron injection into the higher bandgap material [3].

To minimize these effects in AlGaAs/GaAs systems, an aluminum mole fraction x greater than 0.2 is typically used to obtain ΔE_C values of about 0.2 eV [4]. The use of high mole fraction AlGaAs material (x >0.2); however, can lead to three major bad effects [5],[6]. The first of which is the persistent photoconductivity (PPC) due to the high light-sensitivity of GaAs at low temperatures. Second, the observed collapse of the drain current due to DX centers and injection of 2DEG electrons into AlGaAs layer. Third, the uncontrollable threshold voltage shift, commonly noticed in FET devices scaled down to the submicrometer level.

Furthermore, unavoidable secondary effects of the real space transfer [3], which counteracts the confinement of electrons when high field transport is involved, and the generation - recombination noise may also be produced. These effects are of particular importance because they are detrimental to the operation of HEMTs at low temperatures, where these devices offer the highest performance advantages over conventional MESFETs.

In the AlGaAs/InGaAs system, an Al-mole fraction x of only about 0.15 seems sufficient for $\Delta E_C = 0.3$ eV. This low Al-mole fraction allows higher doping densities while avoiding the problems associated with DX- centers occupation, since the density of these traps is significantly reduced. When the device dimensions are scaled down to the submicrometer level, the intrinsic transconductance is determined to a first order by the product of the average electron velocity and the 2DEG capacitance per unit gate length. A higher transconductance is expected with the InGaAs-based systems over the GaAs counterparts due to the higher saturation velocity in InGaAs. Also, the average distance of 2DEG from the interface is smaller due to the improved carrier confinement in the quantum well which provides better control of the gate voltage V_G on the 2DEG concentration.

This paper presents an exact numerical analysis for the 2DEG in both AlGaAs HEMT and PMHEMT, which is based on solving self-consistently both Schrodingr's wave equation and Poisson's equation. The general features of the self-consistent algorithm are explained. Obtained results, such as subband energy levels, conduction band structure, and subband electron distribution, are presented. The numerically calculated data for the charge control is fitted to some analytical expression. A developed analytical model for AlGaAs/ GaAs HEMT, previously introduced[7], has been modified to obtain the current-voltage characteristics and the small signal parameters in PMHEMT. The obtained results have been compared with the available experimental data and revealed an excellent agreement. The PMHEMT performance has been compared with an AlGaAs/GaAs HEMT having identical geometrical and processing parameters, in order to show the great advantages offered by the PMHEMT ,which has become the most popular candidate for high performance HEMTs.

II. Self-Consistent Numerical Analysis

The analysis is based on the numerical solution of Schrodinger's wave equation and Poisson's equation self-consistently. Schrodinger's equation is written as:

$$\frac{d^2\psi_i(x)}{dx^2} + \frac{2m^*}{\hbar^2}[E_i + qV(x)]\cdot\psi_i(x) = 0 \qquad (1)$$

where E_i is the energy level of the i^{th} subband, $\psi_i(x)$ is the corresponding wavefunction, m^* is the effective mass of electrons, $\hbar$ is the reduced Planks constant, and x is the direction normal to the interface into the InGaAs. The conduction band potential $V(x)$ is obtained from the solution of the following Poisson's equation :

$$\frac{d^2V(x)}{dx^2} = -\frac{\rho(x)}{\varepsilon_1} \qquad (2)$$

where ε_1 is the permitivity of InGaAs or GaAs, and $\rho(x)$ is the 2DEG charge density and is determined by the distribution of the electrons $n(x)$ in the 2DEG layer which is given by[8] :

$$n(x) = \sum_i n_i(x) \quad \text{and} \quad n_i(x) = |\psi_i(x)|^2 \cdot N_i \qquad (3)$$

where N_i is the total electron density per unit area of the i^{th} subband and is expressed , assuming a staircase function for the density of states of the 2DEG, as:

$$N_i = \frac{m^*}{\pi\hbar^2} kT \ln\left(1 + \exp\frac{(E_F - E_i)}{KT}\right) \qquad (4)$$

where E_F is the Fermi-level position.

ψ_i is normalized such that

$$\int_{-\infty}^{\infty} |\psi_i(x)|^2 \, dx = \int_0^{\infty} |\psi_i(x)|^2 \, dx = 1 \qquad (5)$$

The total 2DEG density n_S is given by

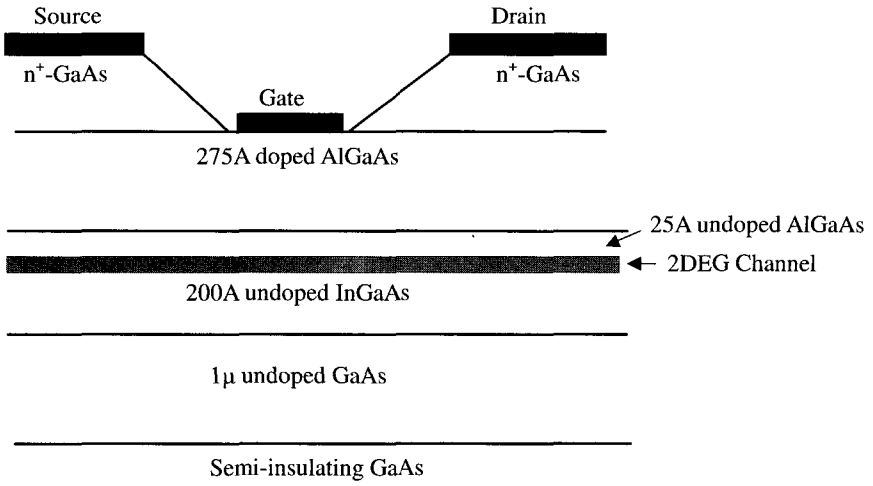

Fig. 1. Schematic cross-section of Pseudomorphic HEMT structure.

$$n_S = \int_0^{\infty} \sum_i n_i(x) dx \tag{6}$$

The differential equations (1) and (2) are solved using Runge-Kutta-Nystrom method [9]. A relaxation method was used rather than attempting a simultaneous solution. The initial conditions for the energy levels E_i, and the potential $V(x)$ are taken from the triangular approximation[10]. The solution starts with an assumed value for the total electron density in the potential well n_S and also for the wavefunction at the heterointerface $\psi_i(0)$. The potential $V(x)$ together with the energy levels E_i are substituted in (1) to calculate ψ_i. An iterative process is continued to update E_i until condition (5) is satisfied. ψ_i (x) is then used to calculate $n(x)$ using (3) -(6). This charge density is eventually substituted into (2) and a new potential distribution is obtained.

The convergence criterion for the energy levels is that the successive eigen values in solving (1), with a given potential distribution, agree to within 10^{-6} eV. While the convergence criterion for the potential is that successive values for $V(x)$ obtained from (2) in successive rounds of iterations, differ by no more than 1 mV. Only three energy subband levels are considered in the analysis. This is because the energy separation between subbands in the InGaAs quantum well are relatively large, hence, more than 99% of the channel electrons are included in the three lowest levels[11].

Fermi-Dirac statistics have been considered in carrying out the solution of (2) in the AlGaAs layer where the ionized donors $N_D^+(x)$, and the free electrons $n_e(x)$ distributions are expressed as:

$$N_D^+(x) = \frac{N_d}{1+2.\exp\left(-(E_C - E_F - E_D)/KT\right)} \tag{7}$$

$$n_e(x) = \frac{4N_C}{1+4.\exp\left((E_C - E_F)/KT\right)} \tag{8}$$

The free electron and the neutralized donor densities, which arise in the AlGaAs at large gate voltage, are calculated by numerically integrating $n_e(x)$ and N_d - $N_D^+(x)$, respectively along the AlGaAs layer thickness.

III. Exact Numerical Results

A typical structure for AlGaAs/InGaAs PMHEMT on GaAs substrate is shown in Fig. 1. The geometrical and processing parameters of the device used for analysis are given in table 1-A. Because of the low Al-mole fraction, x = 0.15, high doping level in AlGaAs layer has been allowed, 3 x 10^{18} cm^{-3} , without increasing the trap density. The conduction band discontinuity ΔE_C at the AlGaAs/InGaAs interface is taken as the sum of two discontinuities of 0.13eV, at the InGaAs/GaAs interface and of 0.11eV at the AlGaAs/GaAs interface[11]. The model and fitting parameters are given in tables 1-B and

Table 1-A. Device Physical Parameters

Parameter	Value	
	Device A	Device B
N_d (cm^{-3}) AlGaAs layer doping	$3x10^{18}$	$3x10^{18}$
D_l (A) AlGaAs layer thickness	275	320
D_i (A) spacer layer thickness	25	40
D_c (A) InGaAs layer thickness	200	170
ΔE_C (eV) AlGaAs/InGaAs conduction band discontinuity	0.24	0.24
ϕ_m (eV) Schottky barrier height	1.0	1.1
ε_2 (F/cm) dielectric constant of AlGaAs	$1.26x10^{-12}$	$1.26x10^{-12}$
ε_1 (F/cm) dielectric constant of InGaAs	$1.31x10^{-12}$	$1.31x10^{-12}$
Z (μm)	145	300
L (μm)	1.0	0.35

Table 1-B. Model Parameters

Parameter	PMHEMT				Conventional		
	2DEG		AlGaAs	Neut. Donors	2DEG	AlGaAs	Neut. Donors
	Device A	Device B					
N_{S0} (cm^{-2})	$9.2 x10^{11}$	$1.16 x10^{12}$	$8.5 x10^{11}$	$1.4 x10^{12}$	$8.7 x10^{11}$	$1 x10^{12}$	$1.5 x10^{12}$
α	0.42	0.52	0.495	0.5	0.475	0.5	0.495
V_m	-0.23	-0.05	0.76	0.39	0	0.73	0.23
V_l	0.4	0.18	0.28	0.11	0.33	0.26	0.075

Table 1-C. Fitting Parameters

Parameter	PMHEMT			Conventional	
	2DEG		AlGaAs	2DEG	AlGaAs
	Device A	Device B			
μ (cm^2/V.s)	6600	6800	1000	5500	1000
V_{sat} ($x10^7$ cm/s)	1.9	2.5	1.0	1.5	1.0
E_S (KV/cm)	3.8	3.5	10	3.8	10

1-C respectively.

Figure 2. shows the conduction band structure, the Fermi-level position, and the positions of the three lowest energy levels. The total electron distribution in the channel as a function of the distance from the interface is indicated in Fig. 3. The contribution of the lowest two subbands is also shown. It is clear that the wide separations between the subband levels result in localized distribution of the 2DEG concentration. Also, a reduced intersubband transition is expected.

The electron density in the InGaAs channel as a function of the applied gate voltage is fitted to the

following analytical function.[12]

$$n_S = n_{S0}\left(\alpha + (1-\alpha)\tanh\left(\frac{V_G - V - V_m}{V_1}\right)\right) \quad (9)$$

where α, n_{S0}, V_m, and V_1 are parameters that best match the numerical data to those obtained from the above analytical expression. Figure 4. shows the good match between the numerical and analytical data. The model parameters are listed in table 1-B.

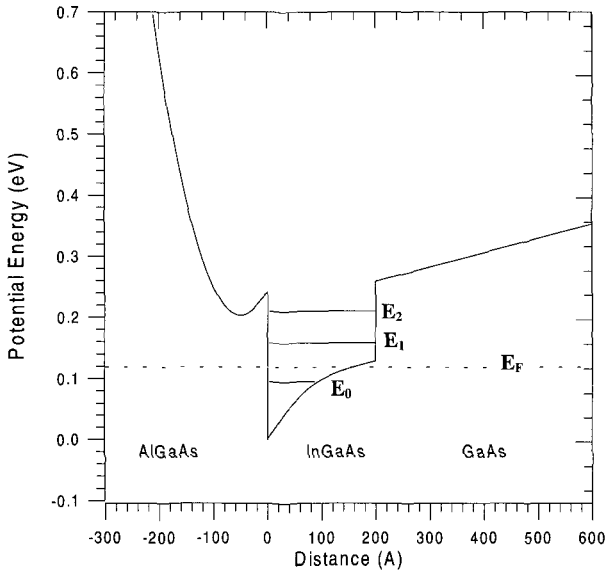

Fig. 2. Model results for conduction band structure, Fermi-level, and the three lowest energy levels for PMHEMT at n_S = 8 x 10^{11}cm^{-2}.

It is worth noting that the carrier concentration in the AlGaAs channel and the concentration of the neutralized donors are also best fit to (9) with different matching parameters. A list of the model parameters is indicated in table 1-B.

IV. Analytical Analysis

Depending on biasing conditions, two channel may be formed in PMHEMT, a 2DEG channel inside the InGaAs layer and a MESFET-like channel in the AlGaAs layer. They both supply carriers for the drain current, so the drain current of the device is a sum of two currents and can be expressed as:

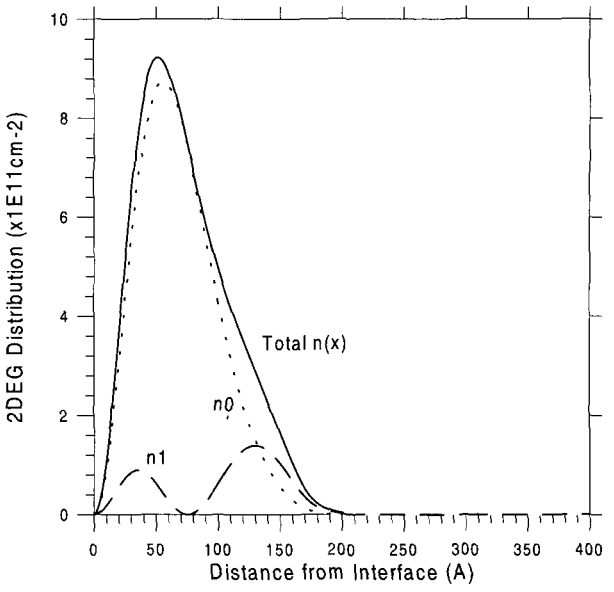

Fig. 3. Total charge distribution in PMHEMT channel at n_S = 8 x 10^{11}cm^{-2}. The contributions of the two lowest subbands are also shown.

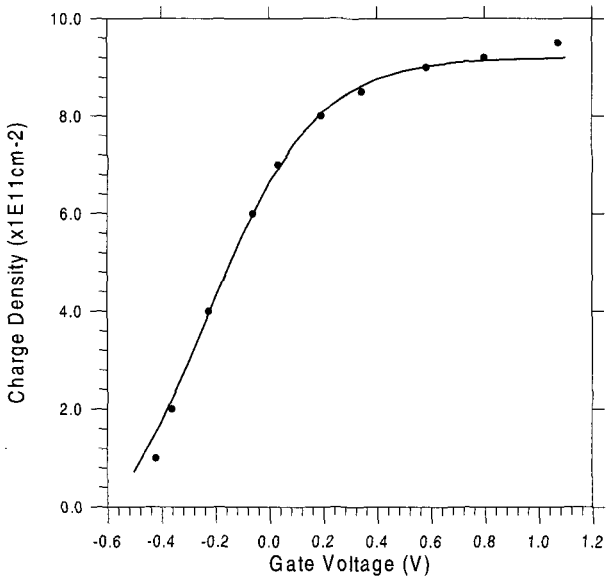

Fig. 4. Charge density in the 2DEG vs. gate voltage. Dots : numerically calculated data. Solid curve : analytical function.

$$I_{Di} = q.Z.n_{Si}.(V_G, V(y)).v_i(y) \quad (10)$$

where V(y) is the channel potential, y is the lateral dimension along the channel, Z is the gate width, $v_i(y)$ is the carrier velocity inside the InGaAs layer, i = 1, or inside the AlGaAs layer, i = 2, and n_{Si} is given by (9).

The following modified two-piece model for the velocity/field relation is assumed[12]:

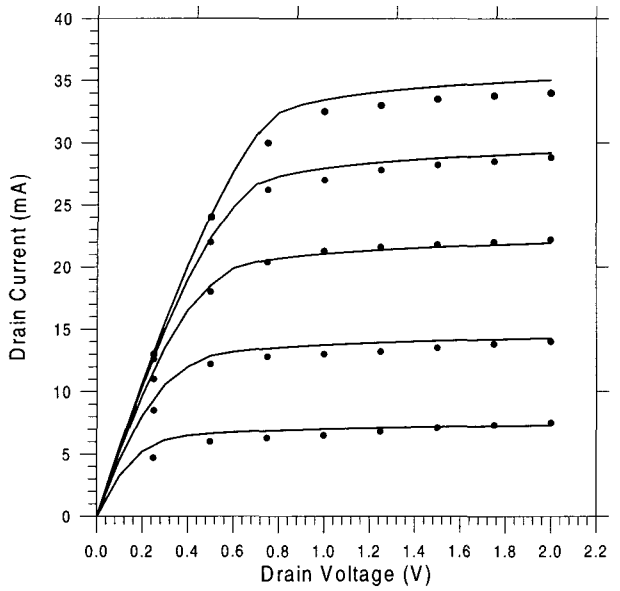

Fig. 5. Model results (solid) for the current-voltage characteristics of PMHEMT, compared with the measured data (dots). The gate voltage ranges from -0.2V to 0.6V in 0.2V steps.

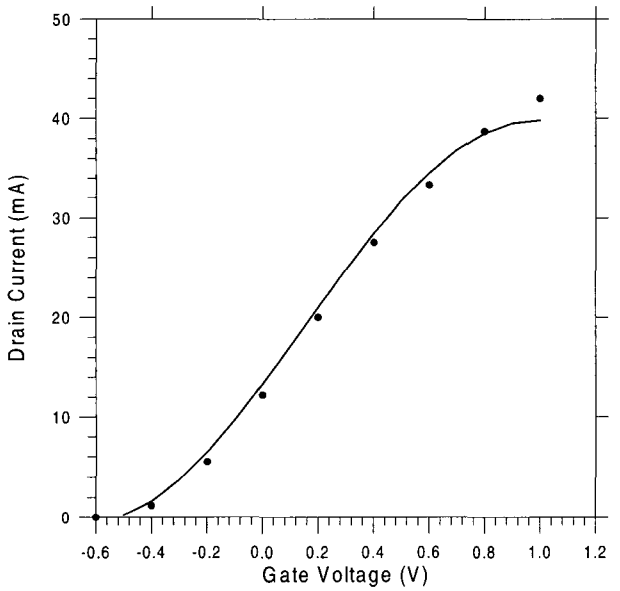

Fig. 6. Transfer characteristics of PMHEMT at V_{DS} = 2V. Dots : measured data, solid curve : model results.

$$v_i(y) = \frac{\mu_i E(y)}{1 + E(y)/E_{1i}} \qquad E(y) < E_{Si}$$
$$= v_{sati} \qquad E(y) > E_{Si} \tag{11}$$

where E(y) is the channel field at a distance y, and E_{Si} is the field inside the channel at which the carriers'velocity reaches its saturation value v_{sati}. The parameter E_{1i} is a constant given by:

$$E_{1i} = \frac{E_{Si}}{\mu_i E_{Si} / v_{sati} - 1} \tag{12}$$

the subscript i always refers to either the channel created inside the InGaAs layer, i =1, or inside the AlGaAs layer, i =2. Table 1-C lists the fitting parameters used in the model.

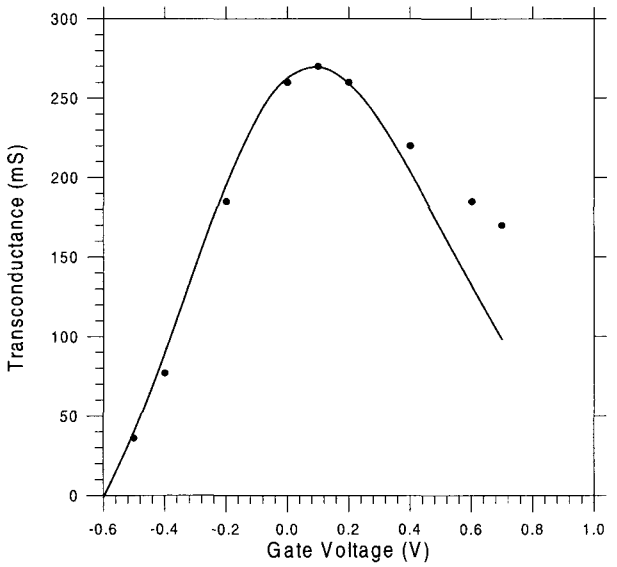

Fig.7. Model results for transconductance vs. gate voltage compared with the measured data (circles).

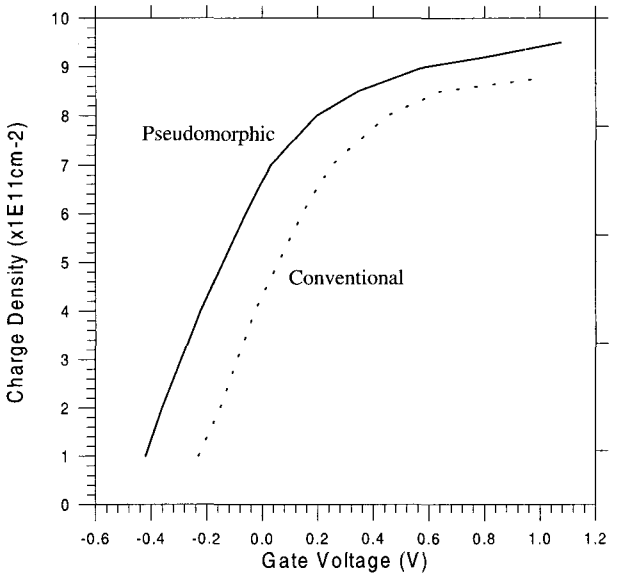

Fig. 8. 2DEG density vs. gate voltage for PMHEMT compared with a conventional HEMT with identical structure.

Replacing E(y) with dV(y)/dy, then substituting (11) into (10) and integrating over the channel length, the drain current results. Based on the two-section model, the linear and saturation darin currents are expressed as[7]:

$$I_{DLi}=\frac{A_i}{L+V_D/E_{1i}}\left[\, B_i\cdot V_D-\ln\cosh\left(\frac{V_G-V_D-V_{mi}}{V_{1i}}\right)+\ln\cosh\left(\frac{V_G-V_{mi}}{V_{1i}}\right)\right] \quad (13)$$

$$I_{DSi}=\frac{A_i}{L_{Ci}+V_{Dsati}/E_{1i}}\left[B_i\cdot V_{Dsati}-\ln\cosh\left(\frac{V_G-V_{Dsati}-V_{mi}}{V_{1i}}\right)+\ln\cosh\left(\frac{V_G-V_{mi}}{V_{1i}}\right)\right] \quad (14)$$

where $A_i=q\mu_i Z n_{S0i}(1-\alpha_i)V_{1i}$, and $B_i=\alpha_i/(1-\alpha_i)V_{1i}$, V_D is the drain voltage, and V_{Dsati} is the channel drain voltage at the onset of saturation [13]. The length L_{Ci} is the distance from the source junction to the point of saturation which lies somewhere along the channel between the source and the drain junctions and is given by:[16]

$$L_{Ci}=L-\frac{2d_t}{\pi}\sinh^{-1}\left[\frac{\pi(V_D-V_{Dsati})}{2d_tE_{Si}}\right] \quad (15)$$

where d_t is the total distance between the gate and the channel.

Differentiating (13) and (14) with respect to V_G, the device transconductance in the linear and saturation regions are obtained as follows:

$$g_{mSi}=\frac{q\mu_i Z}{G_{Li}}(n_{Si}(0)-n_{Si}(V_D)) \quad (16)$$

$$g_{mSi}=\frac{q\mu_i Z}{G_{Li}}\left[n_{Si}(0)+\left(\frac{dV_{Si}}{dV_G}-1\right)n_{Si}(V_{Si})\right]-I_{DSi}\frac{dV_{Si}}{dV_G}EI_i \quad (17)$$

where $G_{Li}=L+\frac{V_D}{E_{1i}}$

$$EI_i=\frac{1}{E_{1i}}+\frac{1}{E_{Si}\cosh\pi(L-L_{Ci})/2d_{ti}},$$

L_{Ci} is the channel length and d_{ti} is the channel width at saturation.

The three components of the total gate capacitance in saturation are given by the following two expressions [7] :

$$C_{ggSi}=\frac{(qZ)^2}{I_{DSi}}\mu_i\left[n_{Si}^2(0)-(1-\frac{dV_{S1}}{dV_G})n_{Si}^2(V_{Si})\right]-\frac{qZ}{E_1}\left[n_{Si}(0)-n_{Si}(V_{Si})(1-\frac{dV_{Si}}{dV_G})\right]+qZ\left[(L-L_{Ci})\frac{dn_{Si}(V_{Si})}{dV_G}-n_{Si}(V_{Si})\frac{dL_{Ci}}{dV_G}\right]-\frac{(qZ)^2}{I_{DSi}^2}\mu_i g_{mLi}\int_0^{V_S}n_{Si}^2dV \quad (18)$$

$$C_{ggS3}=\frac{(qZ)^2}{I_{DS1}}\mu_1\left[n_{S1}(0)n_{S3}(0)-(1-\frac{dV_{S1}}{dV_G})n_{S1}(V_{S1})n_{S3}(V_{S1})\right]-\frac{qZ}{E_1}\left[n_{S3}(0)-n_{S3}(V_{S1})(1-\frac{dV_{S1}}{dV_G})\right]+qZ\left[(L-L_{C1})\frac{dn_{S3}(V_{S1})}{dV_G}-n_{S3}(V_{S1})\frac{dL_{C1}}{dV_G}\right]-\frac{(qZ)^2}{I_{DS1}^2}\mu_1 g_{mL1}\int_0^{V_S}n_{S1}n_{S3}dV \quad (19)$$

where $n_S(0)$, $n_S(V_D)$, and $n_S(V_S)$ are the channel electron densities at the source end, at the drain end, and at the saturation point respectively.

Equation (18) represents the contribution of the 2DEG and the AlGaAs charge components to the gate capacitance (i = 1,2). Equation (19) represents the contribution of neutralized donors component, which is responsible for the rapid increase in the gate capacitance at large gate voltage.

IV. Discussions

The presented model can easily be used to predict the experimental characteristics of both HEMT and PMHEMT devices. The method followed for calculating

the data for both the I-V and the small signal parameters is based on iterative technique developed from the known Runge-Kutta-Nystrom method which has proved to provide fast convergence[9].

To examine the accuracy of the model in predicting the device characteristics and performance, the simulation results are compared with the available experimental measurements [14] of a device whose physical parameters are given in Table 1.A. Figures 5. throurgh 7. show the obtained good agreement between the experimental measurements and the model predictions for the terminal characteristics, the transfer characteristics, and the transconductance of the device respectively.

The performance of the analyzed AlGaAs/InGaAs PMHEMT is compared with a conventional AlGaAs/ GaAs HEMT. The structural parameters of the two devices are identical (table 1.A), except for the InGaAs channel layer which does not exist in conventional AlGaAs/GaAs HEMT, where the 2DEG channel is formed inside the GaAs layer side of the heterointerface. While the parameters of the PMHEMT correspond to a real device[14], the conventional HEMT is purely hypothetical. For simplicity, only the first three subbands, whose energies are calculated self-consistently, are included in the simulation. Figure 8. compares between the sheet electron concentration as a function of the gate voltage for the two devices. A maximum sheet concentration of 9.6 x 10^{11} cm^{-2} is obtained in PMHEMT compared with a value of 8.7 x $10^{11}cm^{-2}$ for conventional HEMT. The threshold voltage V_{th} of the PMHEMT is less than that of the conventional device by about 0.15 V. This threshold voltage difference corresponds to the conduction band discontinuity between InGaAs and GaAs layers (130meV), and the difference between the Fermi-levels in the two devices (21meV) .This result agrees well with the analytical value of V_{th} obtained from the following equation[15] :

$$V_{th} = \phi_m + \Delta E_C - E_F + V_P \qquad (20)$$

where $V_P = \frac{qN_d^2 d_2^2}{2\varepsilon_2}$

Figure 9. shows the transfer characteristics of the PMHEMT as compared with the conventional structure. The figure indicates that the current in the PMHEMT is about two times greater than that of the conventional structure for the same gate and drain voltages. It is important to know that the two devices are precisely the same in terms of geometrical dimensions and doping levels, and the only difference between them is the insertion of the 200 $\mathring{A}$ InGaAs layer in the PMHEMT structure. Therefore, the observed difference in the transfer characteristics arises solely from the different properties of the different materials composing the channel because of the different electron velocities, and the degree of electron confinement within the two-dimensional layer formed in each case.

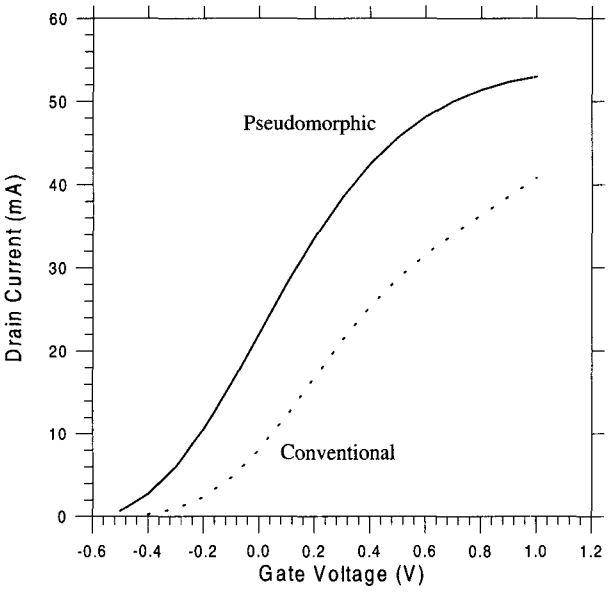

Fig. 9. Transfer characteristics of PMHEMT, compared with that of conventional HEMT with identical structure at V_{DS} = 1.5V.

The transconductance g_m as a function of the gate voltage at a drain bias of 1.5 V (saturation region) is illustrated in Fig.10. It is remarkably noticeable that the maximum value of the transconductance for the PMHEMT is greatly enhanced in comparison with that of the conventional structure. This reflects the increased charge control sensitivity in PMHEMTs.

The intrinsic total gate capacitance C_{gg} at a drain bias of 1.5 V for both devices are shown in Fig.11. The figure indicates that the gate capacitance for PMHEMT shifts towards the negative gate bias. The 2DEG component, which is the main contributor to the gate capacitance at low gate voltage, is higher in the pseudomorphic than in

the conventional structure. The neutralized donors and the free electrons in the parallel channel inside the AlGaAs layer cause the rapid increase of the gate capacitance. The contribution of these two components shifts capacitance values towards the positive gate voltage in PMHEMT, which improves the device performance at higher gate voltages.

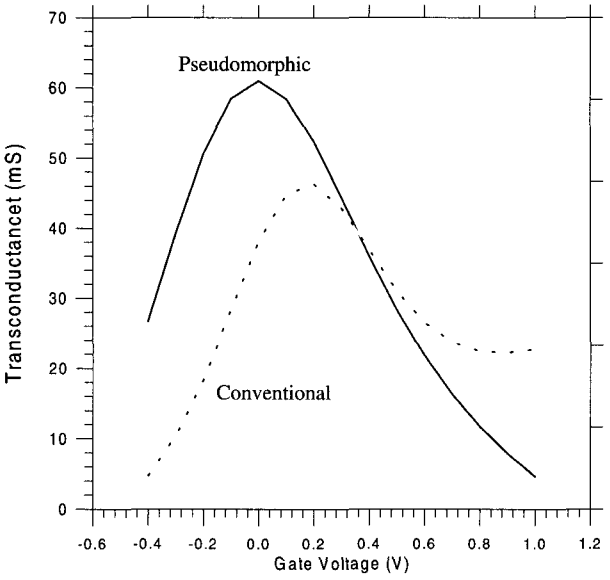

Fig. 10. Transconductance vs. gate voltage for both conventional and PM HEMT HEMTs at V_{DS} = 1.5V.

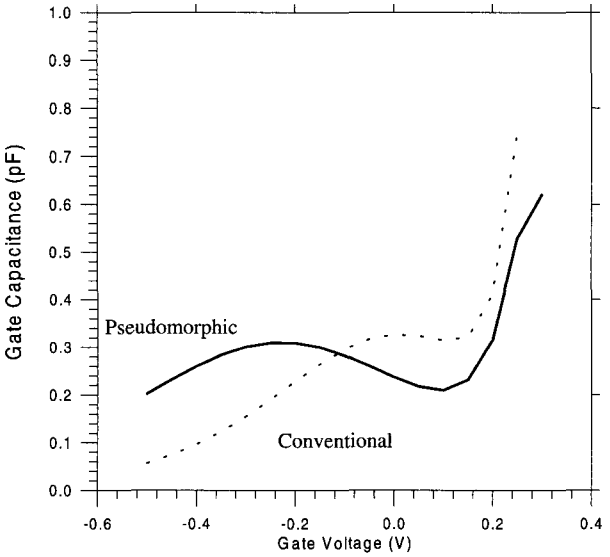

Fig. 11. Total intrinsic gate capacitance characteristics for both conventional and PM HEMT HEMTs at V_{DS} = 1.5V.

The unity current gain cut-off frequency f_T, which is simply given by $f_T = g_m / 2\pi C_{gg}$, as a function of the gate voltage is presented in Fig.12 for the two devices at a fixed drain bias of 1.5 V. It is observed that the maximum value of f_T is approximately two times larger in pseudomorphic HEMT than in conventional GaAs-based HEMT. The calculated value of the cut-off frequency is very near to the experimentally measured value (~46 GHz) [14].

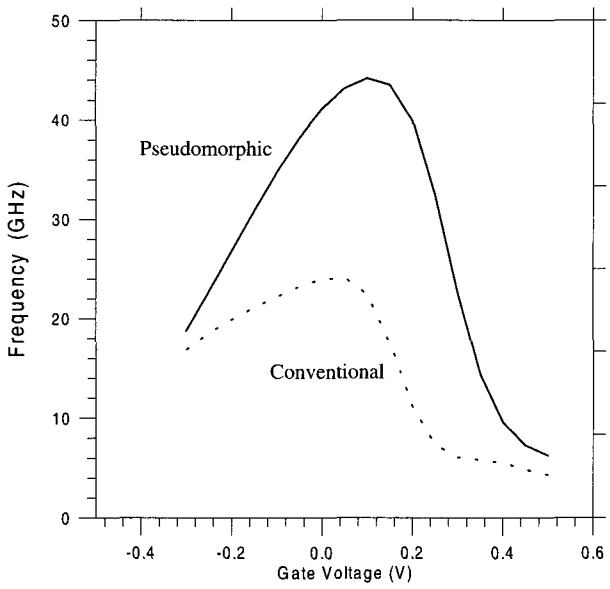

Fig. 12. Unity current-gain cutoff frequency vs. gate voltage at V_{DS} = 1.5V for PMHEMT compared with conventional HEMT.

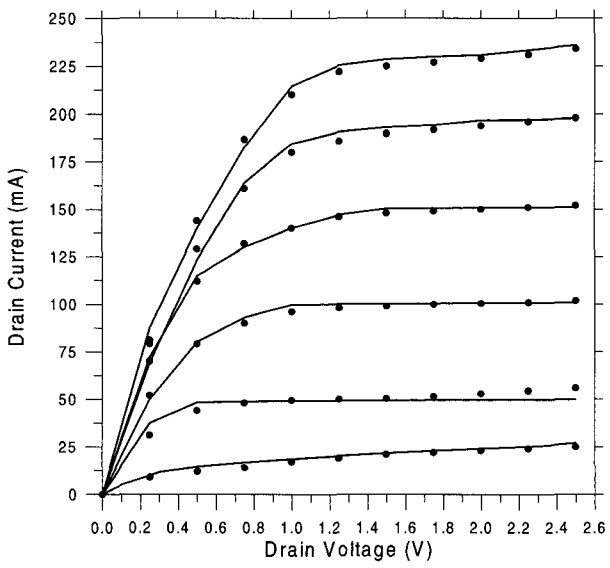

Fig. 13. Model results (solid) for the current-voltage characteristics of a 0.35 μ m gate-length PMHEMT, compared to the measured data (dots). The gate voltage ranges from – 0.2V to 0.8V in 0.2 V steps.

To further confirm the validity of the model in the submicron range, a 0.35 μ m gate-length device, referred to by device B in tables 1A, 1B, and 1C, has been modeled and found to agree well with the experimental results [17] as shown in Fig. 13.

V. Conclusions

A semi-analytical model for PMHEMTs has been presented in this paper. The charge control analysis is based on the simultaneous and self-consistent solution of Poisson's equation and Schrodinger's wave equation. The accuracy of the model has been confirmed through the obtained good match between the theoretical predictions and the experimental terminal characteristics, transfer characteristics as well as the extrinsic transconductance. The model has successfully predicted the gate capacitance over a wide range of biasing voltages. A comparison is made between a competitive conventional HEMT and a PMHEMT which has favored the PMHAEMT in terms of performance and terminal characteristics.

References

[1] F. Diette, D. Langrez, J. L. Cordon, E. Delos, D. Th eon, and G. Salmer "1510 mS/mm 0.1μm gate lengt h pseudomorphic HEMTs with intrinsic current gain cutoff frequency of 220 GHz," Electron Lett. vol. 32, no. 9, pp. 848-850, 1996

[2] K. Lee, M. Shur, T. J. Drummond, and H. Morkoc, "Parasitic MESFET in (AlGaAs/AlGa) modulation do ped FETs and MODFET characterization," IEEE Tra ns. Electron Devices, vol. ED.-31, pp. 29-35, 1984.

[3] K. Hess, "Real space transfer: Generalized approach to transport in confined geometries," Solid-State Electron ics, vol. 31, pp. 329-324, 1988.

[4] K. Park and K. D. Kwack, "A model for the current-voltage characteristics of MODFETs," IEEE Trans. El ectron Devices, vol. ED-33, pp. 673-676, 1986.

[5] N. I. Nathan, "Persistent photoconductivity in AlGaAs/G aAs modulation-doped layers and field effect transistors," Solid-State Electronics, vol. 29, pp. 167-172, 1986.

[6] R. Fisher et *al.*, "On the collapse of drain I-V chara cteristics in modulation-doped FETs, at low temperat ures," IEEE Trans. Electron Devices, vol. ED-31, pp. 1028-1032, 1984.

[7] M. Abdel Aziz, M. EL-Sayed, and M. El-Banna, "An a nalytical model for extrinsic small signal parameters in HEMTs," Solid-State Electronics, vol. 43, pp. 891-900, 1999.

[8] B. Vinter, "Subbands and charge control in two dime nsional electron gas field effect transistor," Appl. Phys. Lett., vol-44, pp. 840-848, 1984.

[9] Kreyszig, "Advanced engineering mathematics," John Wiley & Sons Inc., 1993.

[10] D. Delagebeauduef and N. Linh, "Metal-(n) AlGaAs-Ga As Two dimensional electron GaAs FET," IEEE Trans. Electron Devices, vol. ED-29, pp. 874-881, 1982.

[11] Y. Ando, and T. Itoh. "Analysis of charge control in pseudomorphic two-dimentional electron gas field-effect transistor," IEEE Trans. Electron Devices, vol. ED-35, pp. 2295-2301, 1988.

[12] H. Rohdin and P. Roblen , "A MODFET DC model with Improved pinchoff and saturation characteristics," IEEE Trans. Electron Devices, vol. ED-32, pp. 664-671, 1985.

[13] M. Abdel Aziz and M. El-Banna, "An analytical mo del for AlGaAs/GaAs HEMTs at large gate voltage," 40th MIDWEST Symposium on Circuits and Systems," UC Davis, USA, 1997.

[14] A. Ketterson, et al., "Characterization of InGaAs pse udomorphic modulation doped field effect transistor," IEEE Trans. Electron Devices, vol. Ed-33, pp. 561-571, 1986.

[15] K. Lee et al., "Current-voltage and Capacitance-voltage characteristics of modulation-doped field effect transis tor," IEEE Trans. Electron Devices, vol. ED-30, pp. 207-212, 1983.

[16] A. B. Grebene and S. K. Ghandhi, "General theory f or pinched operation of the junction-gate FET," Solid-State Electronics, vol. 12, pp. 573-589, (1969).

[17] D. H. Park and K. F. Brennan, "Mote-Carlo Simulati on of 0.35 μ m gate length GaAs and InGaAs HEMTs," IEEE Trans. Electron Devices, vol. 37, pp. 618-628 (1990).

Abdel Aziz Khalil was born in Damietta, Egypt in 1954. He received the B. S. and M. S. degrees from the Military Technical College, Cairo, Egypt in 1977 and 1992 respectively. He worked as a Radar and repair engineer in the Egyptian Armed Forces from 1977 to 1989. He received the Ph. D. degree from Alexandria University in 1998. He is currently teaching at the Air Defense College, Alexandria, Egypt. His research interests include semiconductor and microwave devices.

El-sayed received the B. Sc. and M. Sc. Degrees in electrical engineering from Alexandria University, Egypt, in 1975 and 1978 respectively, and the Ph. D. degree from INPG, Grenoble, France, in 1984. Since 1985, he has been with the electrical engineering department, Alexandria University, Egypt, where he is now a professor of Microelectronics. The main area of research of Dr. El-Sayed is the characterization and modeling of semiconductor devices. He also has conducted research works in microwave devices and analog VLSI implementation of neurofuzzy systems

El-Banna (M'89-SM'95) was born in Alexandria, Egypt. He received the B. S. and M. S. degrees in electrical engineering both from Alexandria University in 1979 and 1983 respectively, and the Ph. D. degree from the University of Pittsburgh, USA, in 1988. He is now a professor of electronics with the electrical engineering department at Alexandria University. He was a visiting professor at the United Arab Emirates University at Al-Ain, UAE in 1995. He has been on a leave of absence to Beirut Arab University from 1997 to 2001. His current research areas of interest are modeling and characterization of semiconductor devices for VLSI with special emphasis to HEMTs, PMHEMTs , SOIs and SETs. Dr. El-Banna was designated as a University Scholar for superior academic performance at the University of Pittsburgh, USA in 1985. He served on the Publications Committee of the IEEE-Electron Devices Society in 1996. He has also been a distinguished lecturer for the IEEE-EDS since 1997.